European Journal of Chemistry

View Journal Online
View Article Online

Modification and characterization of selected Zambian clays for potential use as photocatalysts

Mary Mambwe [1], Kennedy Kabaso Kalebaila [1,*], Todd Johnson [2] and John Moma [3]

[1] *Department of Chemistry, School of Mathematics and Natural Sciences, Copperbelt University, 21692, Kitwe, Zambia*
[2] *Department of Biological Sciences, School of Mathematics and Natural Sciences, Copperbelt University, 21692, Kitwe, Zambia*
[3] *School of Chemistry, University of Witwatersrand, Johannesburg, 2001, South Africa*

* *Corresponding author at: Department of Chemistry, School of Mathematics and Natural Sciences, Copperbelt University, 21692, Kitwe, Zambia.*
e-mail: kkalebai@gmail.com (K.K. Kalebaila).

RESEARCH ARTICLE

10.5155/eurjchem.14.3.362-369.2451

Received: 24 May 2023
Received in revised form: 07 July 2023
Accepted: 26 July 2023
Published online: 30 September 2023
Printed: 30 September 2023

KEYWORDS

Clay
Adsorption
Adsorbents
Modification
Zambian clay materials
Photochemical oxidation

ABSTRACT

Natural materials such as clay are valued for their favorable physical and chemical characteristics on the surface. In this study, the selected Zambian clay materials are immobilized with TiO_2 and manganese ions to determine their suitability for use as photocatalysts. SiO_2 and Al_2O_3 oxide composition of Zambian clays was obtained in the range of 35.08-52.63/35.15-52.72 and 13.85-21.73/13.77-21.80, respectively, by inductively coupled plasma (ICP) and X-ray fluorescence (XRF); while Energy dispersive spectroscopy (EDS) of modified clays showed that they have 1.54% incorporation of Ti and 4.98% Mn for Chingola clay to act as UV-Vis absorbers. According to the powder X-ray diffraction analysis of raw clays, the primary phase of all samples is quartz and contains low concentrations of bentonite and kaolinite. The scanning electron microscope (SEM) showed fluffy morphology with agglomeration, while the particle sizes of the clay photocatalysts with the use of transmission electron microscopy (TEM) ranged between 3.0 and 4.8 nm. UV-vis spectroscopy of the samples showed bandgap energies ranging from 2.52-3.08 eV. The surface areas, pore volumes, and pore sizes of the investigated modified and unmodified clays determined by the Brunauer, Teller, Emmett/Barrett Joyner Halenda (BET/BJH) model ranged from 12.06-64.51 m^2/g, 0.029-0.068 cm^3/g, and 0.642-2.802 nm, respectively. To enhance the mixing of oil and clay, the adsorbents were grafted with silane and confirmed by Fourier transform infrared (FTIR) spectroscopy through CH peaks at ~1450 and ~2860 cm^{-1}. The modified clay materials exhibited favorable properties for use as photocatalysts.

Cite this: *Eur. J. Chem.* **2023**, *14(3)*, 362-369 **Journal website**: www.eurjchem.com

1. Introduction

Controlling and preventing environmental pollution is one of the main challenges faced by humans in the modern world. Clay materials have been used for environmental remediation as photocatalysts because they are inexpensive, have a vast surface area, are widely available, are simple to access, are abundant in nature, and are environmentally beneficial. The emphasis on clay is a result of its numerous structural changes, high specific surface area, and chemical stability [1]. Titanium dioxide (TiO_2) is still the most researched photocatalyst in environmental treatments due to its availability, relatively low cost, non-toxic substance with great hydrophilicity, thermal and chemical stability, and photoactivity in ultraviolet or visible light [2]. It is useful as a means to reduce organic pollutants due to its high specific surface, which is caused by nanosized particles and oxidation capacity [3]. Heterogeneous photocatalysis is an improved oxidation technique, and, by using the photochemical oxidation method, many pollutants can be oxidized until they are destroyed. The biggest drawback of using TiO_2 is that it clusters together (agglomerates), making it difficult to remove nanomaterials.

Agglomeration reduces the surface area, which has an influence on the effectiveness of the photocatalyst [4]. Clay materials are among the numerous materials that can be used as alternatives to immobilizing nanomaterials to prevent agglomeration [5]. The process involves immobilizing the titanium particles on the clay surface. The advantages of using TiO_2/clay composites are that they have a large surface area, are inexpensive, and have a high degree of hydrophobicity. Recently, the catalytic oxidation of soil contaminants has been added to the applications of porous materials such as clay [6].

In this study, five clay samples (Chingola, South Luangwa, Mporokoso white, Mporokoso red, Kalulushi) were collected and analyzed by ICP, XRF, and PXRD. However, we only focused on three clay samples (Chingola, South Luangwa and Mporokoso white) because the characteristics are suitable for their use in our further research. These three different Zambian clays were modified with manganese ions and TiO_2 and their characteristics were investigated for potential use as photocatalysts and adsorbents for environmental remediation.

https://dx.doi.org/10.5155/eurjchem.14.3.362-369.2451

Table 1. Relative composition of the major oxides (%) in the five types of clays.

Components	Chingola	South Luangwa	Mporokoso white	Mporokoso red	Kalulushi
SiO_2	52.41	35.08	52.63	41.72	52.36
Al_2O_3	13.89	13.85	21.73	20.22	19.25
Fe_2O_3	4.03	10.35	1.72	4.43	1.64
K_2O	1.11	1.58	4.46	0.10	0.89

Table 2. XRF oxide composition of the different clays in percentage.

Components	Chingola	South Luangwa	Mporokoso white	Mporokoso red	Kalulushi
SiO_2	52.50	35.15	52.72	42.90	52.28
Al_2O_3	14.00	13.77	20.20	21.80	19.27
Fe_2O_3	3.931	10.3	1.673	4.332	1.63
K_2O	1.10	1.52	4.422	0.0966	0.88

2. Experimental

2.1. Preparation and purification of clays

The local clay samples used in the study were collected from the Kalulushi, Chingola, South Luangwa, and Mporokoso areas of Zambia. Clay samples were collected between the cool dry season and the hot and dry season 2021. Upon collection, the clays were purified by the dispersion decantation method [7] to remove impurities and extract the portion of the sample with particles less than 2 µm. The samples were then oven dried at 110 °C for 4 hours to achieve complete evaporation of the moisture. The dried clay was then pulverized using an agitated mortar and pestle and sieved to obtain homogeneous nanoclay particles. Sieve sizes of 355 µm (45 mesh) and 425 µm (40 mesh) were used.

2.2. Modification of clay samples by the sol-gel method

A 50 g sample of each clay (Chingola, South Luangwa, Mporokoso white) was weighed and dispersed in a beaker containing 300 mL of ethanol to make a slurry that was suspended for 24 hours, and the clay slurry was agitated. To the slurry, 10.25 mL acetylacetone as a complexing agent and 1 g $Mn(NO_3)_2$ were added under continuous stirring for 15 minutes. Then, 16.7 mL of $Ti(OPr_4)$ was also added to the reaction mixture. For 24 hours, the mixture was stirred at room temperature to complete the modified sol-gel process. A greenish solution was obtained for South Luangwa clay, a yellowish solution for Chingola clay, and a whitish powder for Mporokoso white clay. The mixtures were then dried in the oven at 80 °C for 6 hours. The materials obtained were then ground and calcined at 550 °C for 3 hours. After calcination, a pinkish powder was obtained for south Luangwa clay, light pink for Chingola, and whitish/grey powder for Mporokoso white clay.

2.3. Grafting of modified clays with isobutyltrimethoxylsilane

Three clay types (South Luangwa, Mporokoso white, and Chingola) were selected based on their suitability for photochemical oxidation. The modified and calcined clay samples were then given an isobutyltrimethoxylsilane treatment, which renders the clay surface hydrophobic and organophilic to fend off water and draw in oil. Making intercalation of numerous polymers requires converting the normally hydrophilic silicate surface to an organophilic one [8]. Trimethoxysilyl-oxy-[-O-$Si(CH_3)_3$] groups are substituted for the OH groups on the clay surface. The surface hydroxyl group of clays and the methoxy group of isobutyltrimethoxysilane form a chemical connection. The modification was carried out as described in the study by Abeywardena *et al.* [8]. Briefly, 10 g of modified and calcined clay was dispersed in ethanol: water mixture (4:1, *v*:*v*) in a round bottom flask at room temperature. 10.75 ml of isobutyltrimethoxylsilane was added dropwise under constant stirring for 24 hours. Subsequently, the mixture was reacted at 110 °C for 3 h. The mixture was then filtered and washed with toluene to remove the unreacted silanes. The surface-modified clays were then dried in an oven at 50 °C for 4 hours.

2.4. Characterization

X-ray fluorescence (XRF, NEX QuantEZ EDXRF) and inductively coupled plasma (ICP, Spectro Arcos), were used to determine the elemental makeup of the clays. X-ray diffraction (PXRD, Rigaku Miniflex 600 Benchtop XRD) was used to examine the crystallinity and phase of natural and modified clay materials using a diffractometer equipped with a spinning copper anode source. The data was generated at a voltage of 40 kV and a current of 150 mA between the ranges of 10 to 70° (2θ). A scanning electron microscope with energy dispersive spectroscopy (SEM-EDS, Zeiss SmartSEM) and a transmission electron microscope (TEM, Philips CM30) were used to assess the morphology of the soils. Ultraviolet-visible diffuse reflectance spectra (UV-Vis DRS) were measured using a Hitach-3900H UV-vis spectrophotometer. Ultraviolet-visible diffuse reflectance spectroscopy was used to assess the optical characteristics of the doped clay samples and the effects of doping on their light absorption. The Brunauer-Emmett-Teller (BET) method was used to determine the specific surface area, and the Barret-Joyner-Halenda (BJH) approach was used to analyze the pore volume and pore diameter by the BET instrument (Microactive TriStar II Plus surface area and porosity analyzer). The adsorption gas used was nitrogen and measurements were taken at 77 K using the Microactive Tristar II Plus surface area and porosity analyzer. Before analysis, the samples were degassed at 100 ° C for approximately 10 hours to remove any molecules that may have been adsorbed. Fourier transform infrared spectroscopy (FTIR) characterization was performed using a Nicolet Avatar TM 360 Fourier transform infrared spectrometer optimized to operate in the 400–4000 cm^{-1} range. KBr/clay-pressed disks were used for the characterization of all clays.

3. Results and discussion

3.1. Inductively coupled plasma (ICP)

The ICP results indicate that all clays were composed mainly of silica and aluminum oxide. The Chingola and Mporokoso white clays had molar ratios of SiO_2/Al_2O_3 of 3.8 and 2.4, respectively, which were more than the kaolinite's predicted molar ratio of 2.00 [9]. Molar ratios that are larger than the theoretical value point to the existence of quartz and other silicates in the samples [10]. The South Luangwa clay had a molar SiO_2/Al_2O_3 ratio of 2.5. According to the literature, materials of type 2/1 (clay with two tetrahedral sheets with one octahedral sheet), such as bentonite, typically correspond to a SiO_2/Al_2O_3 ratio in the range of 2.0-5.5 [11]. The major oxides present in the clay samples are shown in Table 1.

Table 3. *d*-Spacing and crystal size of the investigated clays.

Type of clay	*d*-spacing (Å)		Crystallite size (nm)	
	Unmodified	Modified	Unmodified	Modified
Chingola	4.24	4.23	2.38	1.52
South Luangwa	4.32	4.01	3.27	4.10
Mporokoso white	7.49	7.52	5.49	6.80

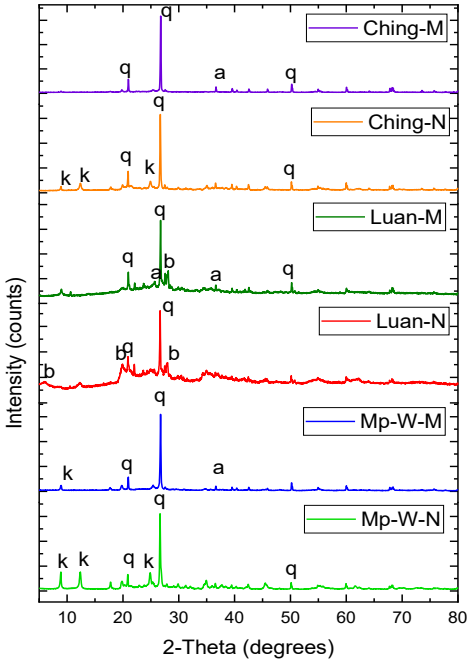

Figure 1. PXRD spectra of the unmodified and modified clays. Ching-M (modified Chingola), Luan-N (natural South Luangwa), Ching-N (natural Chingola), Mp-W-M (modified Mporokoso white), Luan-M (modified South Luangwa), Mp-W-N (natural Mporokoso white), a = anatase, b = bentonite, k = kaolinite, and q = quartz.

3.2. X-ray fluorescence (XRF)

The XRF analysis confirmed the elemental composition of the clays as determined by the ICP analysis. All clays were mainly composed of silica and aluminum as the main constituents, which is also consistent with the results from PXRD, which revealed quartz as one of the components. The percentage composition of SiO_2 and Al_2O_3 ranged from 35.08–52.63 and 13.85–21.73, respectively, and South Luangwa clay had the least SiO_2 and Al_2O_3 while Mporokoso white had the highest SiO_2 and Al_2O_3 content (Table 2).

3.3. Powder X-ray diffraction (PXRD)

The phases were identified by comparing with the pattern of the International Centre Diffraction data (The Joint Committee of Powder Diffraction Standards, or JCPDS) [12]. Powder X-ray diffraction studies showed the crystallinity and phase composition of the natural and modified clay samples. PXRD of the unmodified clays showed that Kalulushi, Chingola, Mporokoso white and Mporokoso red were composed of kaolinite and quartz, while Luangwa clay was composed of bentonite and quartz. The pattern of Luangwa clay reveals a material that is amorphous with a few crystalline phases. The PXRD analyses showed that all clays had high Al/Si levels as seen from the results of XRF and ICP. The results are similar to those found by reference [13]. Figure 1 shows the phases that were observed for the clays from the PXRD analysis.

After alteration, the PXRD spectra of the clays showed no discernible changes; however, elimination of the kaolinite peaks and bentonite was noted. The loss of kaolinite and bentonite peaks (Figure 1, loss of k/b in the spectra of the unmodified clays) could have been caused by cation exchange between Mn^{2+} ions and the interlayer cations during modification. It can also suggest that the change had already occurred [14]. Ti incorporation was also shown by the appearance of the anatase phase. Using the Scherrer equation, the average crystallite sizes of the natural and modified clays were estimated, and they ranged from 2.38-5.49 (unmodified) and 1.52-6.80 nm (modified). The *d spacing* values ranged from 4.24-7.49 and 4.01-7.52 Å for unmodified and modified clays, respecttively (Table 3). Since there were no appreciable differences in the basal spacing of the original and modified clay minerals, it implies that the TiO_2 nanoparticles are not located in the interlayer space of the clays [15,16]. The increase in d-values indicates the successful incorporation of dopants in the clay.

3.4. Scanning Electron microscopy/Energy dispersive spectroscopy (SEM/EDS)

The SEM revealed a fluffy morphology with small asymmetric particles with high levels of aggregation. Micrographs (Figure 2) also showed more porous surface features that could facilitate reactant access to the clay interlayer space and imply better intercalation yield [17]. It was very challenging to structurally identify the morphologies unique to the fundamental clay minerals (kaolinite and bentonite), given the low resolution of the SEM image of this clay, nevertheless, it demonstrates the clay's level of crystallinity. Similar results were obtained by [18]. The amount of impurities (quartz, hematite, *etc.*) in the clay sample affects the particle morphology [9]. Table 4 presents the EDS data for unmodified and modified clays. It can be seen from these data after modification that Ti and Mn ions were successfully incorporated into the clays.

Table 4. EDS data for unmodified and modified clays.

Element	Weight %	Before doping	After doping	
		Atomic %	Weight %	Atomic %
Chingola clay				
O (K)	50.56	66.47	45.58	62.73
Al (K)	17.40	13.57	8.38	6.69
Si (K)	19.68	14.74	33.32	25.56
Fe (K)	9.70	3.65	4.14	1.60
Mn (K)	-	-	1.54	2.24
Ti (K)	-	-	4.98	0.60
South Luangwa clay				
O (K)	46.78	65.42	46.58	62.73
Al (K)	13.09	10.85	6.01	4.99
Si (K)	18.78	14.96	39.28	31.33
Fe (K)	20.10	8.05	5.55	2.40
Mn (K)	-		1.91	0.78
Ti (K)	-		4.75	2.22
Mporokoso white clay				
O (K)	54.40	68.30	49.45	65.41
Al (K)	13.47	10.03	7.53	5.91
Si (K)	24.99	17.87	31.31	23.59
Fe (K)	1.25	0.45	2.70	1.02
Mn (K)	-	-	0.8	0.31
Ti (K)	-	-	6.91	3.05

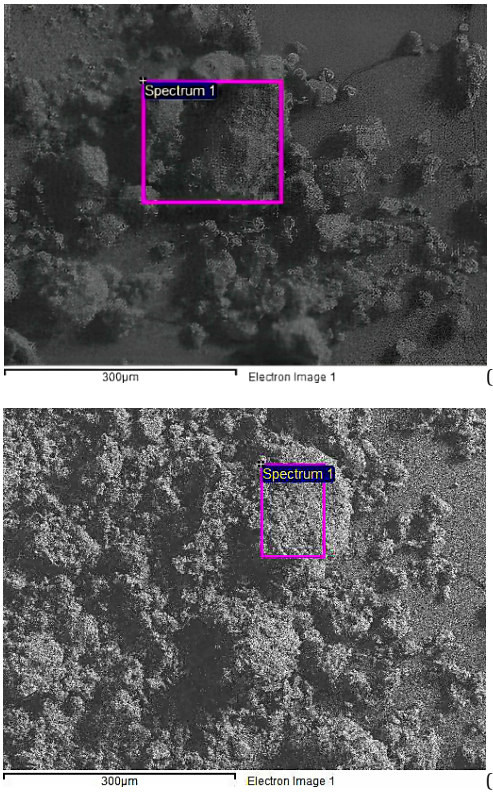

Figure 2. SEM micrographs of (a) natural clays and (b) modified clays for Mporokoso white.

3.5. Transmission electron microscopy (TEM)

Transmission electron microscopy analyzes revealed that the clay particles were mostly spherical in shape as shown in Figure 3. The particle sizes ranged from 3.5–7.0 nm for natural clays and 3.0–4.8 nm for modified clays (Figure 4) and were determined using an image processing program, ImageJ software [19]. A decrease in particle size leads to an increase in the adsorption rate as more adsorption sites are exposed [20].

3.6. Ultraviolet-visible diffuse reflectance (UV-Vis DRS)

Ultraviolet-visible diffuse reflectance was performed to determine the light absorbing capabilities. Bandgap energies for all modified clays calculated from the UV-vis spectrum and compared to the unmodified clays. This indicates that photo-reaction of these modified clays can occur using a light source. The bandgap energies determined by the Kubelka-Munk method [21] were 2.70/2.52, 3.28/3.00 and 3.33/3.08 eV (unmodified/modified) for Chingola, Mporokoso white and South Luangwa clays, respectively.

3.7. Brunauer-Emmett-Teller/Barret-Joyner-Halenda (BET/BJH)

The surface area, pore volume, and pore diameter were studied using the BET/BJH method [22] in the nitrogen adsorption and desorption environment. These particulate properties of the samples are listed in Table 5.

Table 5. Surface area, pore volume, and pore size of the investigated clays.

Sample	Surface area (m^2/g)	Pore volume (cm^3/g)	Pore size (nm)
Natural Chingola	16.7806	0.043	2.266
Modified Chingola	17.9780	0.048	2.376
Natural South Luangwa	50.7037	0.059	0.642
Modified South Luangwa	64.5081	0.068	0.745
Natural Mporokoso white	12.0612	0.029	1.572
Modified Mporokoso white	17.3783	0.038	2.802

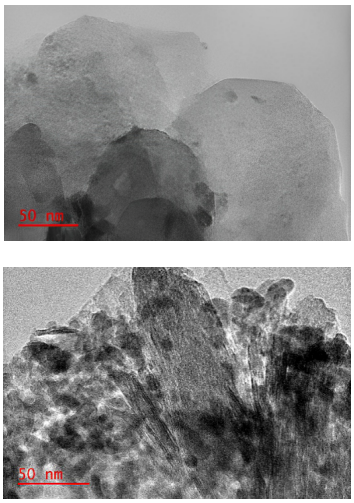

Figure 3. TEM micrographs of (a) unmodified and (b) modified Chingola clays.

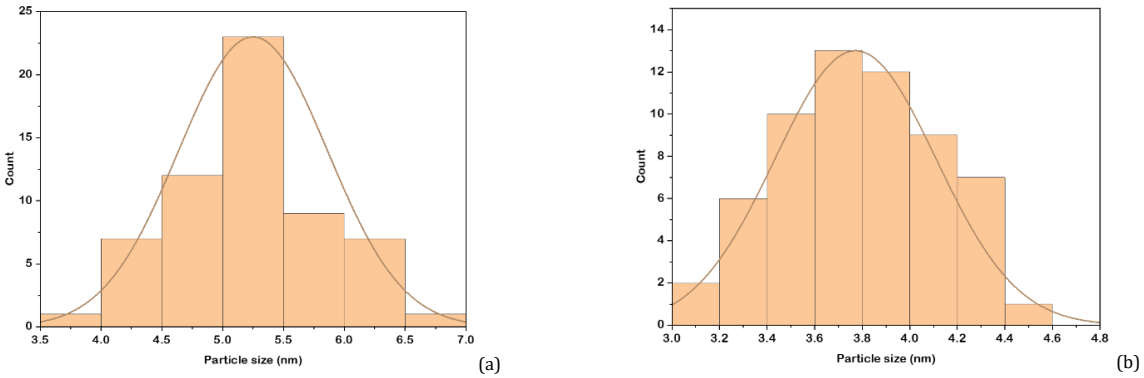

Figure 4. A typical TEM particle size distribution for (a) unmodified and (b) modified Chingola clay.

According to the IUPAC classification [22], all isotherms were type IV isotherms with H3 type hysteresis loops, which is a common curve in mesoporous substances [23]. These phenomena are demonstrated in Figure 5. An increase in the area under the hysteresis loop indicates an increase in the pore size distribution. These isotherms determined the BET surface area, BJH pore volume, and diameter of the clay samples. The desorption branch of the isotherm was used to compute the mesoporous volume using the BJH technique. An increase in surface area, pore volume, and pore diameter was observed in all modified clays compared to the unmodified ones. An increase in the surface area is due to the decreased particle size resulting from the modification process, and it improves the photocatalytic activity by providing more active sites and allowing for more molecules to interact.

3.8. Fourier transform infra-red spectroscopy (FTIR)

The FTIR spectral study identified the functional groups present in the natural and modified clays. Analysis was carried out to identify the various functional groups present that may have arisen from the process of modifying the samples [24]. As an example, FTIR spectra of the unmodified and modified clays of Chingola are shown in Figure 6. Si-O stretching vibrations were observed between 540 and 576 cm^{-1} for all clays showing the presence of quartz (Table 6). The stretching vibrations of the Si-O-Si and Al-O-Al groups linked to the tetrahedral and octahedral leaves are visible in all unmodified clays and appear as distinctive bands at ~910 and ~965 cm^{-1}, respectively. Furthermore, the vibrations of the OH stretching of the structural hydroxyl groups in the clay and water molecules present in the interlayer could be responsible for the bands in the OH stretching region at 3620 and 3629 cm^{-1} found in the FTIR spectra of the raw clays [25].

However, Chingola and Mporokoso white clays have weak bands around 2445 cm^{-1}, which are indicative of the presence of carbonates, such as calcite ($CaCO_3$) or dolomite ($CaMg(CO_3)_2$), and are verified by the presence of CaO and MgO [26]. Furthermore, in all unmodified clays, bands between 530-534 cm^{-1} could be attributed to Si-O-Mg and Si-O-Al [13]. For the modified clays, the peak between 2852 and 2872 cm^{-1} is caused by the hydrocarbon chains of the functional groups of the surfactant. Since the Si-O band (silica) coincides with the CH band of hydrocarbon at ~1235 cm^{-1}, the broadening band at that location indicates the grafting of hydrocarbons on the silica surface [8].

Table 6. FT-IR data (cm^{-1}) for the modified and unmodified clays.

Functional group	Unmodified clays (raw				Modified clays			
	Chingola	South Luangwa	Mporokoso white	Range	Chingola	South Luangwa	Mporokoso white	Range
Si-O-Si	973	921	955	921–973	980	973	976	973–980
Al-O-Al	913	912	908	908–913	-	-	-	-
Si-O-Mg	530	534	534	530–534	-	-	-	–
Si-O-Al	530	534	533	530–534	-	-	-	–
Si-O	576	540	567	540–576	1249	1235	1225	1225–1249
νO-H	3620	3629	3629	3620–3629	-	-	-	–
νC–H	-	-	-	-	2870	2852	2872	2852–2872
δC–H	-	-	-	-	1445	1464	1473	1445-1473

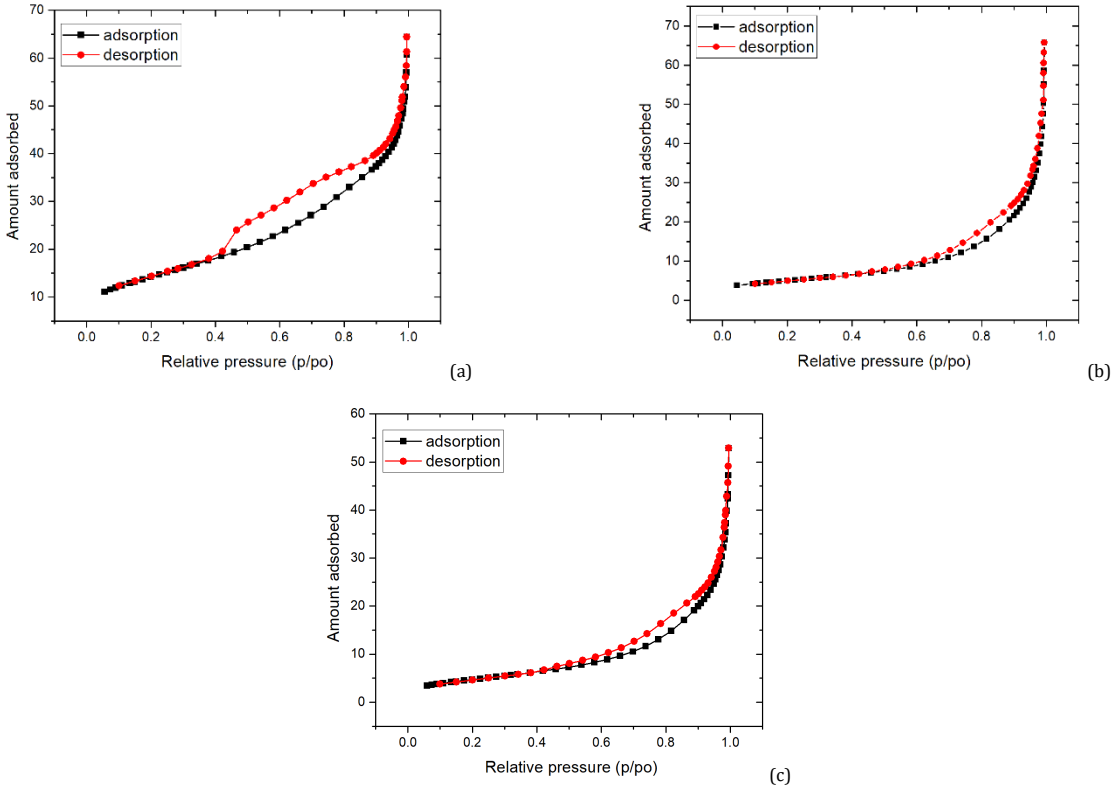

Figure 5. N_2 adsorption desorption isotherms for (a) South Luangwa, (b) Chingola and (c) Mporokoso white modified clays.

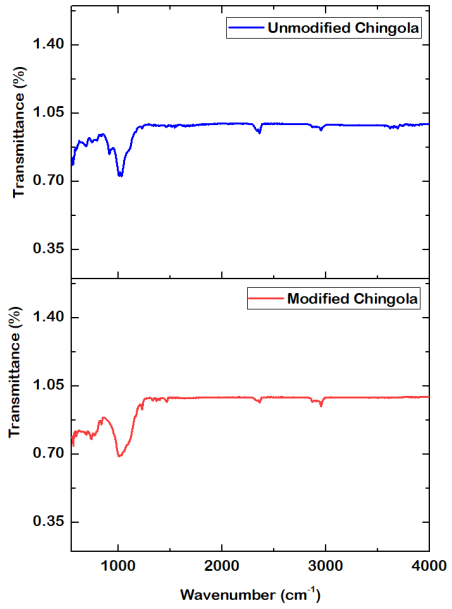

Figure 6. FT-IR spectra for the unmodified and modified Chingola clays.

The existence of bands around 1460 cm^{-1}, which are associated with the bending vibrations of the CH_2 groups in the modified clays, further supports the presence of silane and suggests that the clay mineral has undergone silane modification. This task is consistent with earlier findings by Silva *et al.* [27]. According to Piscitelli *et al*. [24], the existence of bands in the FTIR spectrum that correspond to CH can verify the presence of silane in the structure of the clay mineral. No bonds for Si-O-Ti and Mn ions were detected in all modified clays. Undetected Si-O-Ti bonds in modified clays can result from (1) titanium ions not being embedded in the silica framework or (2) a weak bond between Si-O-Ti and silica [15]. However, it would be predicted that the metal oxide vibrations would be in the same area as Ti and Si vibrations [28].

4. Conclusion

Characterization of the clay samples showed that the components were crystalline and made mainly of kaolinite, bentonite, and quartz. The particles appeared to be fluffy and spherical. The clay samples were mesoporous and had improved light absorption quality. Their surfaces were successfully altered to become hydrophobic or organophilic. The photochemical oxidation properties of selected Zambian clays were determined, and the modified clays have the potential to be used as suitable photocatalysts in the photochemical oxidation of oil in soils contaminated with oil from oil waste and spillage from mining industries in Zambia.

Acknowledgements

The Copperbelt University Africa Centre of Excellence for Sustainable Mining and the Ministry of Technology and Science supported this project. A sincere thank goes to the University of Witwatersrand for providing the SEM, TEM, FTIR, BET/BHJ, and UV-VIS used to generate the required data.

Disclosure statement

Conflict of interest: The authors declare that they have no conflict of interest.
Ethical approval: All ethical guidelines have been adhered to.
Sample availability: Samples of the compounds are available from the author.

CRediT authorship contribution statement

Conceptualization: Mary Mambwe, Kennedy Kabaso Kalebaila, Todd Johnson; Methodology: Mary Mambwe, Kennedy Kabaso Kalebaila, Todd Johnson, John Moma; Software: Kennedy Kabaso Kalebaila, Todd Johnson; Validation: Mary Mambwe, Kennedy Kabaso Kalebaila, Todd Johnson, John Moma; Formal Analysis: Mary Mambwe, Kennedy Kabaso Kalebaila, Todd Johnson, John Moma; Investigation: Mary Mambwe; Resources: Mary Mambwe, Kennedy Kabaso Kalebaila, Todd Johnson, John Moma; Data Curation: Mary Mambwe, Kennedy Kabaso Kalebaila, Todd Johnson, John Moma; Writing - Original Draft: Mary Mambwe; Writing - Review and Editing: Kennedy Kabaso Kalebaila, Todd Johnson; Visualization: Kennedy Kabaso Kalebaila, Todd Johnson; Funding acquisition: Mary Mambwe, Kennedy Kabaso Kalebaila, Todd Johnson, John Moma; Supervision: Kennedy Kabaso Kalebaila, Todd Johnson, John Moma; Project Administration: Mary Mambwe, Kennedy Kabaso Kalebaila, Todd Johnson, John Moma.

ORCID and Email

Mary Mambwe
mambwemary@gmail.com
https://orcid.org/0000-0001-7181-822X
Kennedy Kabaso Kalebaila
kkalebai@gmail.com
https://orcid.org/0000-0003-3561-841X
Todd Johnson
tjforgood@gmail.com
https://orcid.org/0000-0001-6346-5604
John Moma
john.moma@wits.ac.za
https://orcid.org/0000-0002-2345-8087

References

[1]. Mudzielwana, R.; Gitari, M. W.; Ndungu, P. Uptake of As(V) from groundwater using Fe-Mn oxides modified kaolin clay: Physicochemical characterization and adsorption data modeling. *Water (Basel)* **2019**, *11*, 1245.
[2]. Yasmina, M.; Mourad, K.; Mohammed, S. H.; Khaoula, C. Treatment heterogeneous photocatalysis; Factors influencing the photocatalytic degradation by TiO2. *Energy Procedia* **2014**, *50*, 559–566.
[3]. Wongso, V.; Chen, C. J.; Razzaq, A.; Kamal, N. A.; Sambudi, N. S. Hybrid kaolin/TiO2 composite: Effect of urea addition towards an efficient photocatalyst for dye abatement under visible light irradiation. *Appl. Clay Sci.* **2019**, *180*, 105158.
[4]. Hajjaji, W.; Ganiyu, S. O.; Tobaldi, D. M.; Andrejkovičová, S.; Pullar, R. C.; Rocha, F.; Labrincha, J. A. Natural Portuguese clayey materials and derived TiO2-containing composites used for decolouring methylene blue (MB) and orange II (OII) solutions. *Appl. Clay Sci.* **2013**, *83–84*, 91–98.
[5]. Mustapha, S.; Ndamitso, M. M.; Abdulkareem, A. S.; Tijani, J. O.; Shuaib, D. T.; Ajala, A. O.; Mohammed, A. K. Application of TiO2 and ZnO nanoparticles immobilized on clay in wastewater treatment: a review. *Appl. Water Sci.* **2020**, *10*, 49.
[6]. Zhang, X.; Zhang, F.; Chan, K.-Y. Synthesis of titania–silica mixed oxide mesoporous materials, characterization and photocatalytic properties. *Appl. Catal. A Gen.* **2005**, *284*, 193–198.
[7]. González, B.; Pérez, A.; Trujillano, R.; Gil, A.; Vicente, M. Microwave-assisted pillaring of a montmorillonite with Al-polycations in concentrated media. *Materials (Basel)* **2017**, *10*, 886.
[8]. Abeywardena, S. B. Y.; Perera, S.; Nalin de Silva, K. M.; Tissera, N. P. A facile method to modify bentonite nanoclay with silane. *Int. Nano Lett.* **2017**, *7*, 237–241.
[9]. Schackow, A.; Correia, S. L.; Effting, C. Influence of microstructural and morphological properties of raw natural clays on the reactivity of clay brick wastes in a cementitious blend matrix. *Ceramica* **2020**, *66*, 154–163.
[10]. Correia, S. L.; Curto, K. A. S.; Hotza, D.; Segadães, A. M. Clays from southern Brazil: Physical, chemical and mineralogical characterization. *Mater. Sci. For.* **2005**, *498–499*, 447–452.
[11]. Buntin, A. E.; Sirotkin, O. S.; Sirotkin, R. O. Features of the chemical composition and structure of bentonites in Tatarstan. *IOP Conf. Ser. Earth Environ. Sci.* **2022**, *990*, 012041.
[12]. Gates-Rector, S.; Blanton, T. The Powder Diffraction File: a quality materials characterization database. *Powder Diffr.* **2019**, *34*, 352–360.
[13]. Bel Hadjltaief, H.; Ben Ameur, S.; Da Costa, P.; Ben Zina, M.; Elena Galvez, M. Photocatalytic decolorization of cationic and anionic dyes over ZnO nanoparticle immobilized on natural Tunisian clay. *Appl. Clay Sci.* **2018**, *152*, 148–157.
[14]. Mudzielwana, R.; Gitari, M. W.; Akinyemi, S. A.; Msagati, T. A. M. Performance of Mn2+ modified bentonite clay for the removal of fluoride from aqueous solution. *S. Afr. J. Chem.* **2018**, *71*, 15–23.
[15]. Liu, J.; Zhang, G. Recent advances in synthesis and applications of clay-based photocatalysts: a review. *Phys. Chem. Chem. Phys.* **2014**, *16*, 8178–8192.
[16]. Nandiyanto, A. B. D.; Zaen, R.; Oktiani, R. Correlation between crystallite size and photocatalytic performance of micrometer-sized monoclinic WO3 particles. *Arab. J. Chem.* **2020**, *13*, 1283–1296.
[17]. Zaharia, A.; Perrin, F.-X.; Teodorescu, M.; Radu, A.-L.; Iordache, T.-V.; Florea, A.-M.; Donescu, D.; Sarbu, A. New organophilic kaolin clays based on single-point grafted 3-aminopropyl dimethylethoxysilane. *Phys. Chem. Chem. Phys.* **2015**, *17*, 24908–24916.
[18]. Moussa, R. S.; Mamane, O. S.; Habou, I.; Alma, M. M. M.; Natatou, I. Textural, mineralogical and physico-chemical characterization of red clay of Tanout (Zinder-Niger) with a view to its valorization in water treatment. *GSC Adv. Res. Rev*. **2022**, *13*, 039–053.
[19]. Abràmoff, M. D.; Magalhães, P. J.; Ram, S. J. Image Processing with ImageJ. *Biophotonics International 11*, 36–42, https://imagescience.org/meijering/publications/download/bio2004.pdf.
[20]. Kumari, N.; Mohan, C. Basics of clay minerals and their characteristic properties. In *Clay and Clay Minerals*; IntechOpen, 2021, DOI: 10.5772/intechopen.97672.
[21]. Landi, S., Jr; Segundo, I. R.; Freitas, E.; Vasilevskiy, M.; Carneiro, J.; Tavares, C. J. Use and misuse of the Kubelka-Munk function to obtain the band gap energy from diffuse reflectance measurements. *Solid State Commun.* **2022**, *341*, 114573.
[22]. Lopes, J. S.; Rodriguesa, W. V.; Oliveira, V. V, Braga, A. N.; Silva, R. T.; França, A. A.;....Filho, E. C. Modification of kaolinite from Pará/Brazil

region applied in the anionic dye. *Appl. Clay Sci*. **2019**, *168*, 295–303. https://doi.org/10.1016/j.clay.2018.11.028
[23]. Liang, H.; Wang, Z.; Liao, L.; Chen, L.; Li, Z.; Feng, J. High performance photocatalysts: Montmorillonite supported-nano TiO composites. *Optik (Stuttg.)* **2017**, *136*, 44–51.
[24]. Piscitelli, F.; Posocco, P.; Toth, R.; Fermeglia, M.; Pricl, S.; Mensitieri, G.; Lavorgna, M. Sodium montmorillonite silylation: Unexpected effect of the aminosilane chain length. *J. Colloid Interface Sci.* **2010**, *351*, 108–115.
[25]. Eloussaief, M.; Benzina, M. Efficiency of natural and acid-activated clays in the removal of Pb(II) from aqueous solutions. *J. Hazard. Mater.* **2010**, *178*, 753–757.
[26]. Danner, T.; Norden, G.; Justnes, H. Characterisation of calcined raw clays suitable as supplementary cementitious materials. *Appl. Clay Sci.* **2018**, *162*, 391–402.
[27]. Silva, A. A.; Dahmouche, K.; Soares, B. G. Nanostructure and dynamic mechanical properties of silane-functionalized montmorillonite/epoxy nanocomposites. *Appl. Clay Sci.* **2011**, *54*, 151–158.
[28]. Setthaya, N.; Chindaprasirt, P.; Yin, S.; Pimraksa, K. TiO2-zeolite photocatalysts made of metakaolin and rice husk ash for removal of methylene blue dye. *Powder Technol.* **2017**, *313*, 417–426.